Colloids and Surfaces A: Physicochemical and Engineering Aspects 705 (2025) 135603

Contents lists available at ScienceDirect

Colloids and Surfaces A: Physicochemical and Engineering Aspects

journal homepage: www.elsevier.com/locate/colsurfa

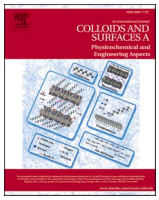

Emulsification in nearly Newtonian and non-Newtonian media of wormlike micelles

Ivan Lesov, Slavka Tcholakova *

Department of Chemical and Pharmaceutical Engineering, Faculty of Chemistry and Pharmacy, Sofia University, Sofia, Bulgaria

GRAPHICAL ABSTRACT

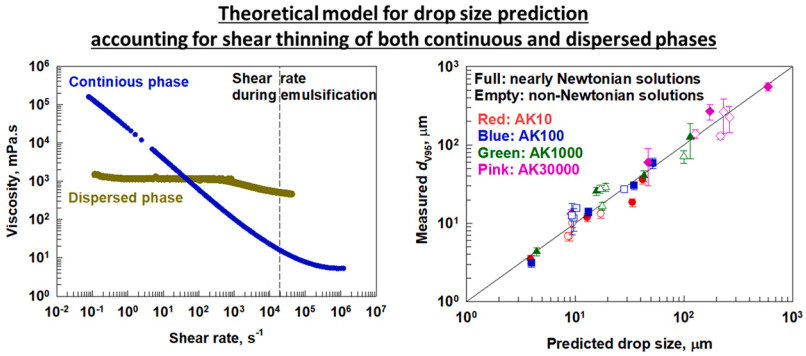

ARTICLE INFO

Keywords:
Emulsification
Drop size
Silicone oils
Non-Newtonian media
Shear thinning
Local shear
Worm-like micelles
Sodium laureth sulfate
Cocoamidopropyl betaine

ABSTRACT

Emulsification experiments with four silicone oils, having viscosities ranging from 0.01 to 30 Pa.s, were conducted in two types of media: nearly Newtonian polyvinyl alcohol (PVA) solutions and non-Newtonian mixtures induced by worm-like micelles in solutions of sodium laureth sulfate and cocoamidopropyl betaine (BS) with NaCl. The increased viscosity of BS solutions upon the addition of NaCl did not significantly affect the drop size in the formed emulsions. In contrast, the increased viscosity of solutions with higher PVA concentrations significantly reduced the drop sizes for all silicone oils. A theoretical expression predicting the maximum drop size in both types of media (nearly Newtonian and non-Newtonian) was derived and validated against experimental data. The expression accounts for shear-thinning behavior in both the aqueous and oil phases. Interfacial stress dominates the breakage of less viscous oils, while viscous stress inside the breaking drop plays a leading role for more viscous oils. The formation of emulsions with similar sizes in non-Newtonian solutions of BS with different NaCl concentrations was explained by their strongly shear-thinning behavior, which leads to nearly similar viscosity at high shear rates, despite their zero-shear viscosities differing by more than two orders of magnitude.

* Correspondence to: Department of Chemical and Pharmaceutical Engineering, Faculty of Chemistry and Pharmacy, Sofia University, 1 James Bourchier Ave., Sofia 1164, Bulgaria.
E-mail address: SC@LCPE.UNI-SOFIA.BG (S. Tcholakova).

https://doi.org/10.1016/j.colsurfa.2024.135603
Received 15 August 2024; Received in revised form 29 September 2024; Accepted 16 October 2024
Available online 18 October 2024

1. Introduction

The drop size distribution in emulsions is an important parameter governing their properties, including visual appearance, stability, rheology, and mouthfeel of edible emulsions [1–5]. In industrial-scale emulsion production, the emulsification usually occurs in turbulent flow [6,7]. The forces responsible for drop breakage depend on the ratio between the size of the breaking drops and the size of the smallest turbulent eddies [8–11]. In the inertial turbulent regime, where drops are bigger than the smallest eddies, the inertial forces are responsible for drop breakage and the viscosity of the continuous phase does not affect drop size distribution [8–11]. In the viscous turbulent regime, where the drops break under the action of viscous forces within the smallest eddies, the viscosity of the continuous phase is a governing factor for effective emulsification [9–12]. Emulsification efficiency is better in the viscous turbulent regime compared to the inertial regime for viscous oils [11]. This is evident by the formation of monodispersed smaller drops and the capability to create emulsions even from highly viscous oils, which may be challenging in inertial turbulence due to their extended deformation time relative to the lifespan of the turbulent eddies [11].

Transitioning from the inertial to the viscous regime of emulsification can be achieved by increasing the overall emulsion viscosity. This can be realized by increasing the oil volume fraction of the dispersed phase [13–16], incorporating synthetic polymers [17–20], utilizing biopolymers [21–24], or increasing surfactant concentrations [15,16,25]. However, most of these strategies lead to non-Newtonian behavior of the continuous phase or of the emulsion as a whole. For example, the concentrated surfactant solutions of individual surfactants, their combinations with zwitterionic surfactants or shorter-chain nonionic co-surfactants with small head groups, exhibit non-Newtonian behavior [26–30]. Introducing salt to these solutions results in the formation of worm-like micelles, with a zero-shear viscosity peaking [27,28,30] at a given salt concentration. Further increases in salt concentration led to the formation of branched micelles, exhibiting a different rheological response compared to that observed before the maximum [27–30]. The impact of the presence of worm-like micelles and their branching on the emulsification ability remains unclear and it is one of the aims of the current study.

In recent years, there has been an increased interest in the flow characteristics of non-Newtonian fluids [31–33]. Studies have revealed that the stress near the wall is significantly higher in non-Newtonian fluids compared to Newtonian fluids, both in microchannels [33] and in turbulent flow within rotor-stator mixers [31]. Notably, the breakage of rape-seed oil drops in turbulent flow within microchannels was observed to be slower in xanthan solutions exhibiting non-Newtonian behavior compared to water [32]. This observation led to the suggestion that the shear-thinning rheology of the continuous phase hinders the dynamics of successive breakup events [32].

In a previous study [21], we established that the incorporation of biopolymers, such as modified starch, serves to increase the viscosity of the continuous phase, consequently enabling the formation of nano-emulsions from triglyceride drops. In this study, we proposed a theoretical expression for predicting the drop size in the formed emulsions. While the viscosity of emulsifying media is well-defined in systems exhibiting a Newtonian rheological response, the use of non-Newtonian fluids introduces a challenge in determining which viscosity parameter to consider for drop size prediction.

Here, we focus on developing a new theoretical model to predict drop size in emulsions formed from both nearly Newtonian and non-Newtonian fluids. The model will allow researchers and practitioners to choose the energy-efficient method for the preparation of advanced materials based on emulsions. Specifically, solutions of polyvinyl alcohols (PVA) were employed as representatives of nearly Newtonian fluids, while a mixture of sodium laurethsulfate (SLES) and cocoamidopropyl betaine (CAPB), denoted as BS in the text, was used as a model for non-Newtonian media [29,30]. The salt concentration was varied for the BS solution to increase the viscosity by inducing micellar growth before the maximum and the formation of branched micelles after the maximum. Notably different rheological characteristics are established for these systems before and after the maximum [29].

Silicone oils are widely used in various cosmetic and personal care products [34–39], such as body washes and conditioners, as well as in drug delivery systems, antifoam production, etc. In most of these applications, the silicone oils are emulsified as drops in different media, and the stability of the formed products depends significantly on the drop size [39]. In the current study the emulsification of silicone oils with viscosities ranging between 0.01 and 30 Pa.s is performed. To interpret the outcomes of emulsification experiments, the shear viscosity as a function of shear rate is measured using two different methods - namely, a rotational rheometer and diffusive wave spectroscopy. Additionally, the interfacial tension is obtained through the utilization of a drop volume tensiometer and drop shape analysis. The obtained results are compared with theoretical expressions proposed in the literature and expressions are modified to account for the shear thinning behavior of aqueous and oily phases.

2. Materials and methods

2.1. Materials

For the preparation of nearly Newtonian solutions, Polyvinyl alcohol with a molecular mass of 205 kDa and 88 % degree of hydrolysis (PVA 40-88, product of Fluka) was used. The solutions were prepared by measuring the necessary amount of PVA and dispersing it in water. The prepared dispersion was allowed to hydrate for approximately 2 h at 70–80 °C, after which it was cooled down to room temperature during continuous mixing and used within the same day.

For the preparation of non-Newtonian fluids, we used sodium laureth sulfate, SLES (Steol CS270, Stepan, 70 % activity) with IUPAC name of Poly(oxy-1,2-ethanediyl)-alpha-sulfo-omega-(dodecyloxy)-sodium salt, and cocamidopropyl betaine, CAPB (Tegobetain F50, Evonik, 40 % active) with IUPAC name of 2-[(3-dodecanamidopropyl)dimethylaminio]acetate, and sodium chloride (Teokom, Bulgaria, analytical grade). The total concentration of SLES and CAPB in the used solutions for emulsification experiments was fixed at 10 wt% at 2:1 wt:wt ratio for SLES and CAPB. The surfactant mixture is denoted hereafter as BS. For solutions containing NaCl, the following procedure was used – the necessary amount of surfactant was calculated and diluted with water. After complete dissolution, the solid NaCl was added directly to the mixture and mixed for 1–2 h to ensure homogeneity. For example, 100 g BS with concentration 10 wt% BS + 4 wt% NaCl was made the following way: 6.667 g SLES and 3.333 g CAPB were diluted to 96 g by deionized water and 4 g NaCl were added after their dissolution.

All aqueous solutions were prepared with deionized water with resistivity > 18 MΩ.cm, purified by Elix 5 module (Millipore).

As an oily phase, silicone oils from Wacker, Germany (AK10, AK100, AK1000, and AK30 000) with different viscosities were used without any further purification.

2.2. Emulsion preparation

Emulsions were prepared by adding 2 g of oil to 18 g surfactant solutions, which roughly corresponds to 10 vol% of the oily phase, because the mass density of silicone oil is close to that of water [34]. Emulsions were homogenized in 50 mL glass beakers for 5 min at 18,200 rpm with a rotor-stator homogenizer (Ultra Turrax, IKA).

The homogenizer was equipped with an S10N - 10G Dispersing tool (rotor diameter of 7.465 mm and gap of 380 ± 50 μm between the rotor and the stator). The global shear rate was estimated by $\dot{\gamma} = 2\pi rN/l$, where r is the rotor radius ($r = 3.7325$ mm for our equipment), N is the rotation speed (set to 303 rotations per second), and l is the gap-width between the rotor and stator (380 ± 50 μm) and the estimated global

shear rate is $\dot{\gamma} \approx (1.87 \pm 0.25) \times 10^4\ s^{-1}$. The average rate of energy dissipation during emulsification was estimated by $\varepsilon = b_1 N^3 L^2$, where $b_1 = 6$ [13]; $N = 303$ rps and L is a rotor diameter, which is 7.465 mm. Thus, $\varepsilon \approx 9.3 \times 10^3\ m^2/s^3$.

Emulsification was held at an ambient temperature: of 25 ± 3.5 °C. To avoid overheating beyond this point during emulsification in viscous fluids, e.g. 10 wt% PVA, we used a water bath set at 25 ± 1 °C. Subsequently, the samples were taken for optical observation via microscope Axioplan (Zeiss, Germany) utilizing a long-distance objective Zeiss Epiplan 50 ×/0.40. For each sample, at least 3000 drops were measured, and the mean volume (d_{v50}) and maximum (d_{v95}) diameters were determined. Samples for observation were taken during the final seconds of homogenization and diluted in pure water for 10 wt% BS or in 1 wt% BS for PVA. The emulsions were measured, using glass slide and cover glasses (two cover glasses as spacers and one put on top of them as cover, allowing sample thickness of 170 μm).

The emulsions were stored after preparation for up to 6 h before measuring the drop size by laser diffraction (Analysette 22, Fritsch). Prior to measurement, the emulsions were manually stirred and around 1 mL were taken and injected directly into the wet cell unit, where they were in situ diluted by water. The emulsions were gently mixed by the equipment pump, set at rate 3 with ultrasound turned off. At least two independent measurements were made per sample with typical variation of the maximum sizes < 10 %.

2.3. Dynamic and equilibrium interfacial tension

Dynamic interfacial tension was assessed at 25 °C via Drop Volume Tensiometer (DVT50, Krüss GmbH). The injection of oil drops into surfactant solutions at rates ranging from 1 to 200 μL/min was used to measure the dynamics of the adsorption of surfactant at short times. The average surface tension from 2 to 3 drops at characteristic times were taken and plotted against the average surface age of the drop (surface age is defined as the time between two drops detaching from the capillary and passing through the detector). The capillary used for the measurement was with a diameter of 0.254 mm and no corrections were applied to the conventional model as suggested by the equipment manufacturer.

Drop shape analysis (DSA30, Krüss GmbH) was used for equilibrium interfacial tension measurements. A U-shaped capillary was used for measuring oil drops in aqueous solutions at 25 °C. The densities of the aqueous solutions were measured using a densitometer (DMA 35, Anton Paar), and oil densities were used as provided by the manufacturer. At least two measurements were made per concentration. Modification of the method with rapid drop injection was used and referred to as Fast Deformed Drop Method (FDDM). For its use, we applied automated drop injection with speeds up to 1250 μL/min for 1 mm capillary for PVA and 1.5 mm for BS solutions respectively.

2.4. Viscosity characterization

Viscosity at 25 °C was assessed utilizing two different methods: (a) a rotational rheometer (Anton Paar, MCR e302), equipped with cone and plate geometry (40 mm cone diameter, 1° angle), which was used to measure the apparent viscosity at low shear rates ranging from 1 to 2000 s^{-1} or up to the shear rate where the sample was ejected due to inertia; (b) Diffusive wave spectroscopy (DWS, LS instruments) was employed for the measurement of the complex viscosity at high frequencies via monodisperse polystyrene particles with diameter of 780 nm for BS and PVA solutions or TiO_2 nanoparticle tracers for the oils with diameter of 360 nm. 1 mL samples were diluted with 0.05 μL PS particle suspension (10 wt%) or 0.04 g TiO_2 solid particles. Afterward, the suspensions were homogenized manually via stirring with a spatula. The suspensions were put in 5 mm thick glass cuvettes and measured at 25 ± 0.1 °C, ensuring that the sample thickness over the mean free path of the particles, is within the recommended limits between 5 and 40. Typical measurement was carried at 600 s + 180 s Echo, where at least 3 repetitions were performed. For less viscous oils, e.g. AK10 and AK100, particle sedimentation was observed at longer times, so we used shorter measurements: 180 s + 30 s Echo with additional homogenization between the runs.

3. Experimental results and discussions

3.1. Rheological response of used solutions and oils

The rheological behavior of silicone oils with varying viscosities, PVA solutions with different polymer concentrations (C_P), and 10 wt% BS solutions with varying salt concentrations (C_S), used in emulsification experiments, is analyzed using two complementary techniques: rotational rheometry and Diffusive Wave Spectroscopy (DWS). The apparent viscosity is defined as the measured shear stress divided by the applied shear rate and is determined in shear ramp experiments via a rotational rheometer. The complex viscosity as a function of angular frequency, ω [rad/s], is measured in DWS experiments.

According to the Cox-Merz rule [40], the apparent viscosity is equal to the complex viscosity when the shear rate matches the angular frequency. Numerous studies confirm that this semi-empirical equation applies to various systems such as polymeric gels [40–43], worm-like micelle solutions [44], emulsions [45], and bijels [46]. However, evidence suggests that the Cox-Merz rule may not apply to heterogeneous fluids, such as particle suspensions and associating polymers [47–50].

To verify the applicability of the Cox-Merz rule to our systems, we plotted the experimental data for apparent and complex viscosities as functions of shear rate and angular frequency in Figs. 1 and S1. For all silicone oils (AK10, AK100, AK1000, and AK30000), the viscosities measured by the two methods closely align in regions where shear rates and angular frequencies overlap, confirming that the Cox-Merz rule is valid. Notably, even AK1 000 000 was found to obey this rule [51]. The measured shear viscosities for silicone oils are close to those given by the producer [34].

The viscosities of PVA solutions with C_P of 1 wt% and 3 wt% measured by both methods are similar, as illustrated in Fig. S1. However, PVA solutions with higher concentration show systematic deviation: the complex viscosity measured by DWS is ≈ 2-times lower than the apparent viscosity measured by the rotational rheometer, Fig. S1. Such deviation was previously observedfor 16 wt% PVA solution, and the effect was attributed to enhanced interchain associations in shear [52] via the formation of more intramolecular hydrogen bonds between polymer molecules when shear aligns their chains [53]. It was shown [54] that flow affects the relaxation spectrum by shifting the curve to shorter times under steady shear [54]. For predicting the drop breakage, the polymer behavior in shear flow at a high shear rate is important. We assumed that the experimental data from DWS could be used to predict shear-thinning behavior in shear flow after appropriate matching (offsetting), as illustrated in Fig. S1 in the SI. The matching is necessary for having the information for the shear-thinning behavior of PVA solutions at high shear rates.

The viscosities of BS ± NaCl solutions, measured by both methods overlapped, thus conforming to the Cox-Merz rule. This effect was supported by previous studies on worm-like micelles by DWS [55]. It should be noted that the tracer particles aggregated with time with the BS in the absence of salt, and only the first measurements at shorter times were used.

We assume that the viscosity relevant to the emulsification experiments is the viscosity obtained at the high shear rates, i.e. the complex viscosity from the DWS. However, as there are some deviations between the two methods for the PVA solutions, we compare the theoretical predictions using both methods in the upcoming sections.

It should be noted that the measured complex viscosity at high frequencies is not exactly equal to the shear viscosity, as the elastic component predominantly characterizes the response at high

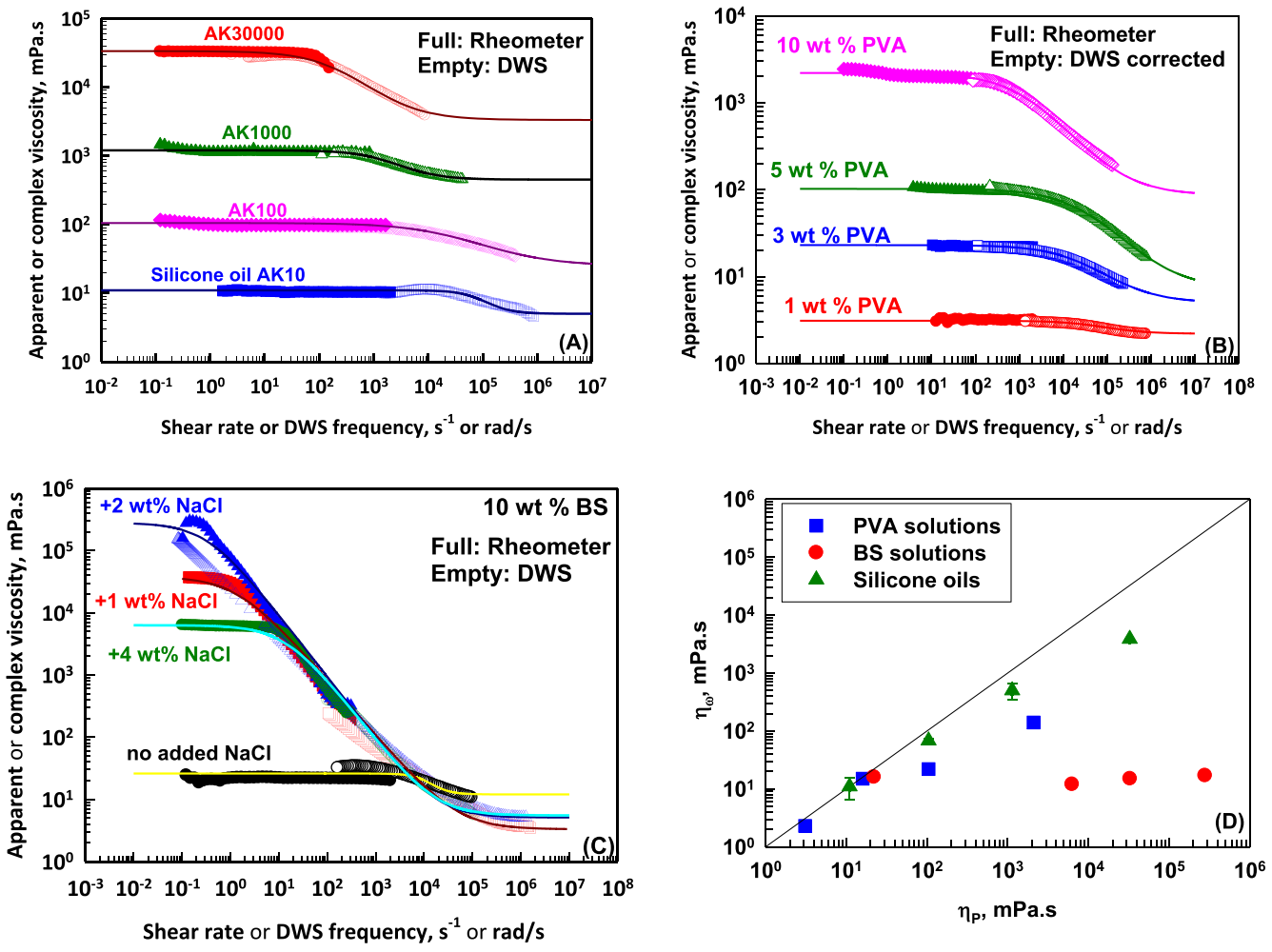

Fig. 1. (A–C) Apparent viscosity (full symbols) as measured by rotational rheometer and complex viscosity (empty symbols) as measured by DWS as a function of shear rate in the rheometer or DWS frequency for (A) Silicone oils; (B) PVA solutions and (C) BS solutions at different salt concentration; (D) Complex viscosity, η_ω, determined from DWS measurements at $\omega = 1.9 \times 10^4$ rad/s as a function of the apparent viscosity, η_P, measured for same system in rheometer at plateau region. The curves in (A-C) are the best fit of experimental data according to Eq. (1). The experimental data for PVA solutions obtained in DWS are corrected to match the data obtained by the rheometer.

frequencies. However, we used these results to obtain at least some information on how the viscosity changes at high shear rates. For BS±NaCl solutions, the expected decrease in shear viscosity with increasing shear rate, based on theoretical considerations [56,57], aligns with the experimental data obtained from DWS measurements, which justifies the approach used.

The viscosity for all studied systems remains constant for a certain range of shear rates/frequency of oscillations and decreases afterward which is typical non-Newtonian behavior. The measured viscosities are fitted by using the Cross model [58,59] which was originally derived for the dependence of apparent shear viscosity on shear rate, but as explained above the used rheometer is not able to assess the high shear rates which are important for drop breakage and that is why we use the results from DWS for complex viscosity as a function of angular frequency:

$$\eta = \eta_\infty + \frac{\eta_0 - \eta_\infty}{1 + (k\omega)^n} \quad (1)$$

here η_0 is the zero-shear viscosity, η_∞ is the viscosity at high values of ω, k is the characteristic time which is related to the critical ω at which complex zero-shear viscosity starts to decrease and n is the slope of viscosity decrease in the intermediate region. The parameters determined from the best fits are summarized in Table 1 together with the values of complex viscosity, η_ω, at $\omega = 1.9 \times 10^4$ rad/s and of shear viscosity at plateau region, η_P.

The determined values for apparent viscosity at low shear rates for BS solutions containing different salt concentrations are in very good agreement with the results reported by Mitrinova et al. [29], where it was shown that the addition of CAPB to SLES solutions dramatically increases the zero-shear viscosity of these solutions due to the formation of very long worm-like micelles. As a consequence, the zero-shear viscosity of the BS solution in the presence of 2 wt% NaCl increases up to 280 Pa.s, as shown in Mitrinova et al. [29]. The full characterization of BS solutions is given [29]. In this study we showed that the BS solutions behave as typical solutions containing worm-like micelles and the increase of salt concentration to 4 wt% leads to formation of branched micelles which have much lower zero-shear viscosity compared to micelles formed at 2 wt% salt (6.3 Pa.s vs 280 Pa.s).

3.2. Interfacial properties of used solutions

Interfacial tension is another key parameter in emulsification. The experimental data for the interfacial tension of AK10 and AK100 in PVA and BS solutions are given in Fig. 2. Interfacial tension of the PVA solutions decreases from ≈ 27–24 initially to 21–18 mN/m at 300 s corresponding to the total time for emulsification. The interfacial tension for BS solutions started at 6–4 mN/m and decreased to about 4 mN/m

Table 1
Comparison of apparent viscosity measured by rotational rheometer at plateau region, η_P with complex viscosities from DWS, η_ω determined at $\omega = 1.9 \times 10^4$ rad/s. The parameters from the fit with Cross rheological model (Eq. (1)).

System	η_P, mPa.s	η_ω, mPa.s	Parameters in Eq. (1)			
			η_0, mPa.s	k, s	n	η_∞, mPa.s
AK10	11	11	11	1.1×10^{-5}	1.75	5
AK100	105	68	105	3.3×10^{-5}	0.65	25
AK1000	1140	500	1200	5.5×10^{-4}	1.10	450
AK30000	32,700	3870 3950*	33,500	5.0×10^{-3}	0.88	3330
1.25 wt% PVA	3.1	2.3 2.8**	2.5 3.1**	1.4×10^{-5} 1.4×10^{-5}**	0.86 0.86**	1.7 2.2**
3 wt% PVA	23	15	23	3.5×10^{-5}	0.70	5.0
5 wt% PVA	105	22 62**	50 102**	9.4×10^{-5} 3.2×10^{-5}**	0.64 0.67**	5.0 7.3**
10 wt% PVA	2100	140 393**	1200 2200**	2.9×10^{-3} 7.3×10^{-4}**	0.81 0.68**	90.0 86.5**
10 wt% BS	22	16	26	8.4×10^{-5}	2.12	12
BS + 1 wt NaCl	33000	15	38400	0.7	0.9	3.3
BS+2 wt% NaCl	280000	17	280000	3.0	1.0	5.1
BS + 4 wt% NaCl	6300	12	6300	0.07	1.0	5.5

* Digitized producer data, as from Ref. [34].
** Parameters after applying matching procedure for data obtained from rheometer and DWS.

with the addition of salt. The increase detected at short times in the DVT was previously related to hydrodynamic effects from the drop pinch-off volume, as observed in Refs. [60,61].

The 10 wt% PVA solutions could not be measured in the DVT due to the high continuous phase viscosity. For the same reason, the solution with BS was reduced to 5 wt%, instead of the 10 wt% that were used for emulsification.

3.3. Results from emulsification experiments

The maximal drop diameter, d_{V95}, the mean volume drop diameter, d_{V50}, and the polydispersity index (PDI) are shown in Fig. 3, while the drop volume distributions for both the PVA and the BS emulsions are shown in Figs. S2 and S3, respectively. Here the polydispersity is defined as PDI $= ((d_{V84}\text{-}d_{V19})/2d_{V50})^2$.

AK10 is effectively emulsified in all PVA and BS solutions. Increasing the PVA concentration from 1.25 wt% to 10 wt% leads to 10-fold decrease in d_{V95} (from 36 ± 4 to 3.5 ± 0.4 μm) and an 8-fold decrease in d_{V50} (from 14.7 ± 1.6 to 1.8 ± 0.3 μm). Additionally, there is a 2.9-fold decrease in thePDI from 0.43 to 0.15, indicating that higher concentrations of PVA lead to the formation of smaller, more uniform drops. Although AK10 is also successfully emulsified in BS solutions, the effects of adding NaCl and the resulting increase in apparent viscosity at low shear rates have a less pronounced impact on drop size distribution. For example, adding 2 wt% NaCl to the BS solution, which increases the apparent viscosity by more than 10^4 at low shear rates, results in a 2-fold reduction in d_{V95} (from 13.2 ± 2.0 to 6.8 ± 0.8 μm) and a 1.5-fold reduction in d_{V50} (from 6.1 ± 0.6 to 3.5 ± 0.4 μm), and a decrease in PDI (from 0.25 to 0.08). Thus, the increase in PVA concentration affects significantly more the emulsification of AK10 compared to the addition of NaCl to BS solutions.

AK100 is effectively emulsified in BS solutions and in PVA solutions with a concentration of 3 wt% or higher, where the maximal drop size remains below 30 μm. However, a secondary peak in drop size distribution is seen for emulsions formed in 1.25 wt% PVA solution, as shown in Fig. S2B. Increasing the PVA concentration to 3 wt% reduces the presence of larger drops, although two distinct peaks still appear in the histogram. Emulsions with a monomodal distribution are formed from PVA solutions with higher concentrations. Specifically, increasing the PVA concentration from 1.25 wt% to 10 wt% leads to a 19-fold reduction in d_{V95} (from 59 ± 9 to 3.1 ± 0.4 μm), a 17-fold decrease in d_{V50} (from 29 ± 4 to 1.7 ± 0.3 μm), and a 5-fold reduction in the PDI from 0.72 to 0.14. Adding 2 wt% NaCl to BS solution results in a 3-fold decrease in d_{V95} (from 27 ± 4 to 11 ± 1.2 μm) and d_{V50} (from 14.7 ± 1.6 to 5.1 ± 0.6 μm), with a slight reduction in PDI from 0.24 to 0.16.

Increasing the viscosity of the silicone oil to AK1000 results in the formation of very large drops when using a 1.25 wt% PVA solution, as illustrated in Fig. S2C. Emulsions with a bimodal distribution are formed with 3 and 5 wt% PVA, while monodisperse emulsions are obtained with 10 wt% PVA solutions. Emulsions formed in BS solutions also exhibit a secondary peak in drop size distribution but with a smaller contribution.

Emulsification of AK30000 is challenging in PVA solutions with concentrations up to 5 wt%, but almost monodisperse emulsions are formed with a 10 wt% PVA solution. In BS solutions, the emulsions with two distinct peaks are formed, as shown in Fig. S3D. The first peak's maximum is at sizes of approximately 5 μm, while the second peak appears at sizes of about 80 μm. These emulsions are highly polydisperse, with a PDI above 1, as shown in Fig. 3.

Experimental data presented in Fig. 3 demonstrate that both d_{V95} and

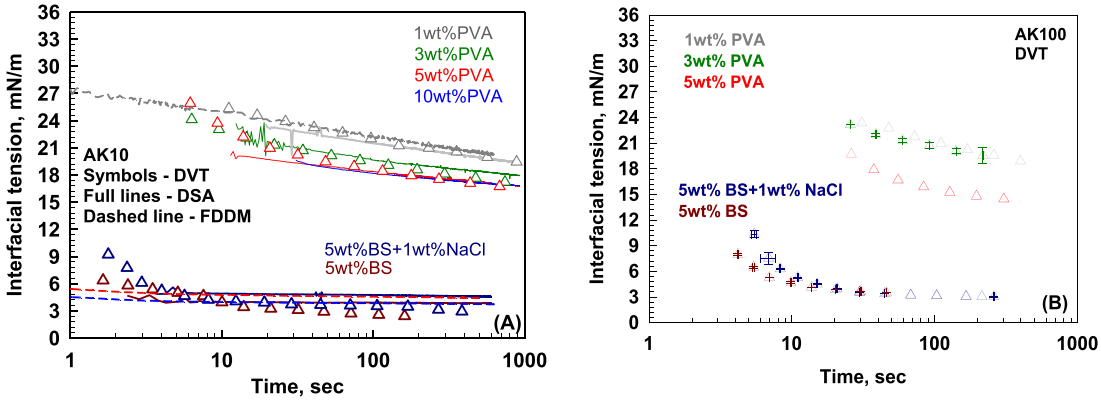

Fig. 2. Interfacial tension as a function of time for PVA and BS solutions for (A) AK10 and (B) AK 100. Solutions are measured via DVT (symbols), via DSA (full lines), and FDDM via dashed lines.

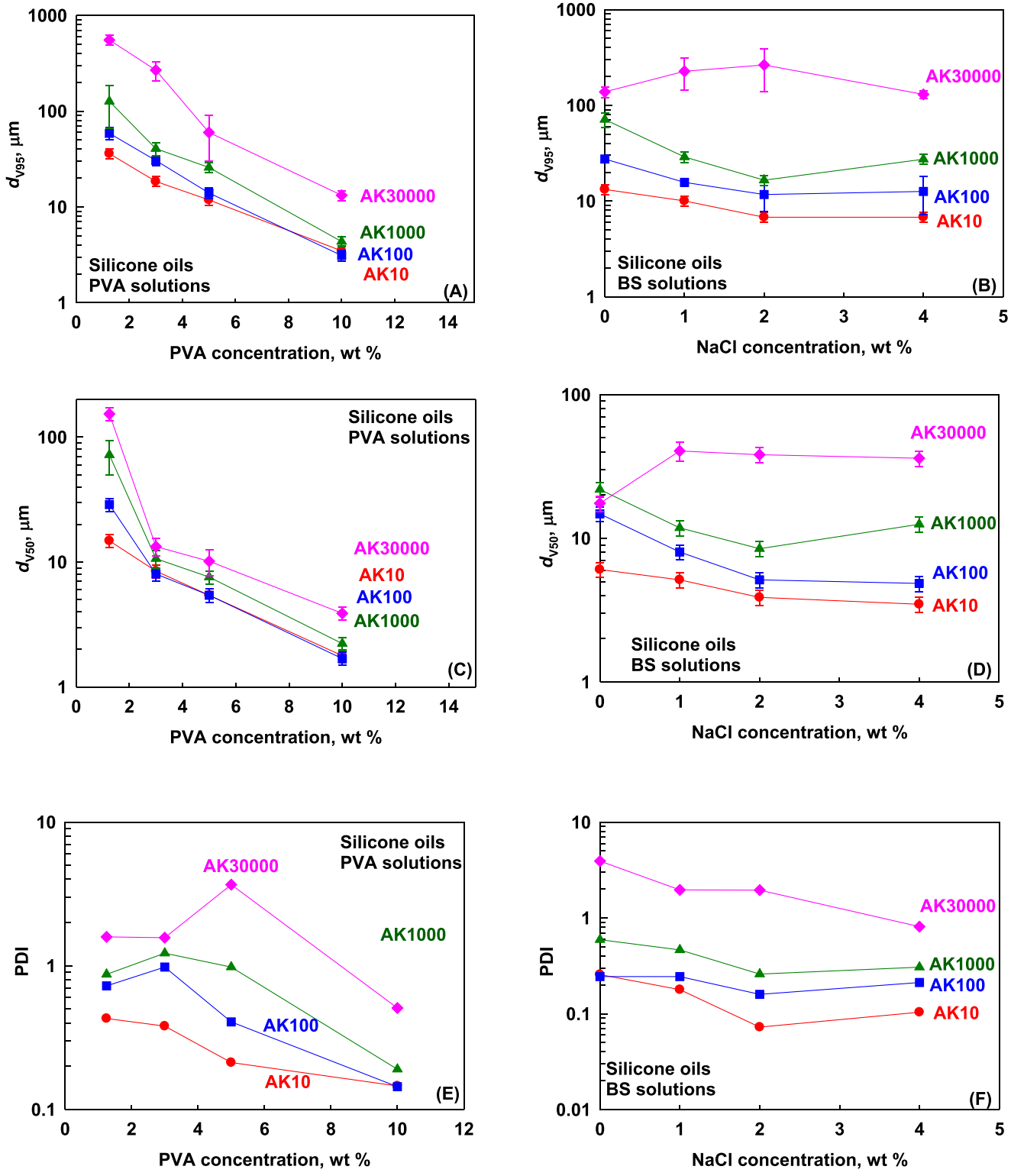

Fig. 3. (A, B) Maximal drop diameter, d_{V95}; (B, D) Mean drop diameter, d_{V50}; (E, F) Polydispersity index, PDI for silicone oil emulsions formed in (A, B, E) PVA solutions with different concentrations and (C, D, F) 10 wt% BS solutions with different NaCl concentrations.

d_{V50} decrease with increasing PVA concentration. At a given concentration of PVA, the values for d_{V95} and d_{V50} are higher for more viscous oils. The PDI remains almost constant up to 5 wt% PVA and decreases significantly when 10 wt% PVA is used for emulsification. Increasing NaCl to 2 wt% in BS solutions reduces the drop sizes and the PDI of the emulsions formed. However, further increasing NaCl to 4 wt% has no effect or results in a slight increase in drop sizes for AK1000 emulsions.

3.4. *Interpretation of the experimental results*

To interpret the data, we used the following approach: (1) Determine the regime of emulsification by comparing the size of the smallest eddies

with experimentally determined value of d_{V95}; (2) Compare the experimental data for d_{V95} for inertial regime of emulsification with theoretical predictions; (3) Compare the experimental data for d_{V95} obtained in turbulent viscous regime with results from "Grace plot" (4) Propose new equation for prediction the outcome of emulsification in both inertial and viscous turbulent flows after accounting for shear thinning behavior of continuous and disperse phases.

The size of the smallest eddies, λ_0, in turbulent flow provides a measure of the length scale at which inertial and viscous forces are equal [9,10]. At distances larger than λ_0, inertial forces dominate, whereas at shorter distances, viscous forces prevail. The inertial force is directly linked to fluctuations in the hydrodynamic pressure within the flow, which are in turn proportional to fluctuations in turbulent velocity. According to the Kolmogorov-Hinze theory, the expression for the fluctuations of the hydrodynamic pressure in the flow is given by [9,10]:

$$\langle \Delta P_T(\lambda_0)\rangle = C_1\rho_C\langle U^2\rangle = C_1C_2\rho_C(\varepsilon\lambda_0)^{2/3} \quad (2)$$

In Eq. (2), the brackets mean statistical averaging, $\langle U^2\rangle = C_2(\varepsilon d)^{2/3}$ is the mean square of the fluctuations in the fluid velocity at distance λ_0, and $C_{1,2}$ are numerical constants calculated by Batchelor [62] to be $C_1 \approx 0.7$ and $C_2 \approx 2.0$, ρ_C is the mass density of the continuous phase, while ε is the rate of energy dissipation per unit mass of the fluid [J/kg.s], which for used hydrodynamic conditions is 9.3×10^3 m^2/s^3.

The viscous forces are proportional to the viscous stress [62], which in turn depends on the shear rate and the viscosity of the continious phase. For Newtonian fluids, the viscosity does not depend on the shear rate, but for non-Newtonian fluids it does. The shear rate inside the smallest turbulent eddies is given by [9,10]:

$$\dot{\gamma}_{\lambda_0} = C_2^{1/2}\frac{(\varepsilon\lambda_0)^{1/3}}{\lambda_0} \quad (3)$$

The size of the smallest eddies is determined from the equalization of the pressure fluctuations given by Eq. (2) and viscous stress inside the smallest eddies, which is expressed for Newtonian fluid as [9,10]:

$$\tau_V = \eta\dot{\gamma}_{\lambda 0} \quad (4)$$

where η is the viscosity of the continuous phase, which does not depend on the applied shear rate for Newtonian fluid.

For continuous phase having non-Newtonian behavior, the viscosity depends on shear rate as shown in Fig. 1. Eq. (1) accounts for this shear thinning behavior and that is why it can be used instead of constant shear viscosity which leads to following expression for viscous stress inside the smallest turbulent eddies in non-Newtonian media:

$$\tau_V = \eta_\infty\dot{\gamma}_{\lambda 0} + \frac{\eta_0 - \eta_\infty}{1 + (k\dot{\gamma}_{\lambda 0})^n}\dot{\gamma}_{\lambda 0} \quad (5)$$

After equalization of viscous stress given by Eq. (5) and pressure fluctuations, given by Eq. (2) and substituting $\dot{\gamma}_{\lambda 0}$ in Eq. (5) by expression given in Eq. (3) the following expression for size of the smallest turbulent eddies in Newtonian and non-Newtonian fluids is derived:

$$C_1C_2\rho_C(\varepsilon\lambda_0)^{2/3} = \left(\frac{\eta_{C0} - \eta_{C\infty}}{1 + \left(k_C C_2^{\frac{1}{2}}\frac{(\varepsilon\lambda_0)^{\frac{1}{3}}}{\lambda_0}\right)^{n_C}} + \eta_{C\infty}\right) C_2^{1/2}\frac{(\varepsilon\lambda_0)^{1/3}}{\lambda_0} \quad (6)$$

For Newtonian liquids, Eq. (6) is simplified to well-known expression for λ_0 [9,10]:

$$\lambda_0 = C_1^{-3/4}C_2^{-3/8}\rho_C^{-3/4}\eta_C^{3/4}\varepsilon^{-1/4} \approx \rho_C^{-3/4}\eta_C^{3/4}\varepsilon^{-1/4} \quad (7)$$

Table S1 presents the calculated values of λ_0 for various solutions used in emulsification experiments, derived under three different assumptions: λ_{01} is calculated using Eq. (6), which accounts for the shear-thinning behavior of the fluids; λ_ω is determined by Eq. (7), assuming a constant viscosity equal to the viscosity measured by the DWS at $\omega = 1.9 \times 10^4$ rad/s, corresponding to the global shear rate; λ_P is also calculated by Eq. (7), but it assumes the viscosity of the continuous phase is equal to the zero-shear viscosity measured by the rheometer.

The shear rates within the smallest eddies in all three assumptions are calculated using Eq. (3) above. Note that Eq. (3) simplifies for Newtonian fluids to the widely used expression for estimating shear rate within the smallest turbulent eddies [8,9,63,64]. The shear rate estimated using Eq. (3) for 1.25 wt% PVA is approximately five times higher than the estimated global shear rate (8.1×10^4 s^{-1} vs 1.87×10^4 s^{-1}). Increasing the PVA concentration leads to a significant decrease in shear rate within the smallest turbulent eddies, which becomes lower than the global shear rate for 10 wt% PVA solutions (6.9×10^3 vs 1.87×10^4 s^{-1}).

It is observed that for solutions exhibiting nearly Newtonian behavior - such as 1.25 and 3 wt% PVA, as well as 10 wt% BS - the values of λ_0 calculated using the three different viscosities are similar. However, for non-Newtonian solutions, λ_0 values vary significantly based on the viscosities used for calculations. The greatest variation occurs in the 10 wt% BS + 2 wt% NaCl solution, where the highest change in the viscosity was observed with $\lambda_P > 3000 \times \lambda_{01}$. The shear rate inside the smallest eddies also varies with the viscosity of the continuous phase. The larger the value of λ_0 the smaller the shear stress inside the smallest turbulent eddies as should be because the total stress remains constant and equal to pressure fluctuations in the inertial regime.

The comparison between the estimated values of λ_0 and the experimentally measured values of d_{V95}, shown in Fig. S4, suggests that emulsification occurs in the inertial regime when using a 1.25 wt% PVA solution and in the viscous regime with a 10 wt% PVA solution. For emulsions formed in 3 and 5 wt% PVA solutions, the size of the drops closely matches the calculated values of λ_0, suggesting that the emulsification occurs mostly in the viscous regime. The emulsification behavior in BS solutions is notably more complex due to larger variations in λ_0, but it is seen that $\lambda_P > d_{V95}$ which means that the emulsification at least in some parts of the equipment occurs in the viscous regime.

For all emulsions prepared in the inertial regime with 1.25 wt% PVA, the PDI exceeds 0.4, indicating that the breakage of a single drop results in daughter and satellite drops of varying sizes. This observation is in unison with previous results, which demonstrated that more viscous oils emulsified in the inertial regime tend to produce polydisperse emulsions [65]. Successful emulsification in the inertial regime depends on two conditions: (1) the duration of pressure fluctuations, which are characterized by lifetime of eddies, must exceed the drop deformation time. This requirement is particularly crucial when dealing with viscous oils; (2) the pressure fluctuations must be higher than the sum of the capillary pressure and the viscous stress inside the breaking drops;

The deformation time in the inertial regime is estimated by [6]:

$$t_{DEF} = \frac{\eta_D}{5\varepsilon^{2/3}d^{2/3}\rho_C} \quad (8)$$

The lifetime of eddies is given by:

$$t_{EDDY} = \frac{d^{2/3}}{\varepsilon^{1/3}} \quad (9)$$

The minimal drop size that can be emulsified in the inertial regime can be defined from the requirement $t_{DEF} \le t_{EDDY}$ and it is given by:

$$\frac{\eta_D^{3/4}}{5^{3/4}\varepsilon^{1/4}\rho_C^{3/4}} \le d_{MINI} \quad (10)$$

The calculated values of the minimal drop size in the inertial regime, d_{MINI}, that can be deformed during the lifespan of the eddies with similar size, are shown in Table S2. These calculations are performed by using two different viscosities of the disperse phase $\eta_{d\omega}$ and η_{DP}. Data in Table S2 show that the measured d_{V95} of 550 ± 60 μm for AK30000

emulsified in 1.25 wt% PVA is significantly smaller than the calculated by Eq. (10) when using the shear viscosity measured from the rheometer (2340 μm). The calculated value of d_{MINI} from Eq. (10) using $\eta_{d\omega}$ is 472 μm which is very similar to one measured experimentally. This comparison clearly shows that along with the shear thinning behavior of the continuous phase, the decreased viscosity of the dispersed phase has to be accounted for proper determination of the drop size of very viscous oils such as AK30000.

The second requirement for drop breakage in the inertial regime leads to the equation proposed by Davies [8]:

$$C_1 C_2 \rho_C (\varepsilon d_I)^{2/3} = C_4 \frac{\sigma}{d_I} + C_5 \eta_D C_2^{1/2} \frac{(\varepsilon d_I)^{1/3}}{d_I} \quad (11)$$

In our previous study [11] we showed that the combination of the constants $C_4/C_1C_2 = 0.86$ [11], which means that $C_4 = 1.089$; and $C_2^{1/2}C_5/C_4 = 0.37$, thus $C_5 = 0.285$. The application of above equation for emulsions formed in 1.25 wt% PVA which have interfacial tension of 27.2 mN/m with AK10 and 28.3 mN/m with AK100 gives the values of d_{IP} given in Table S2 when viscosity of the dispersed phase is the one measured by the rheometer. Note that for AK1000 and AK30000 the interfacial tension has negligible effect on the predicted value of d_{IP} because of dominating contribution of viscous stresses inside the breaking drop (second term in right-hand side of equation). That is why for AK1000 and AK30000 we use the same interfacial tension as one measured for AK100. The estimated values of d_{IP} for AK10 and AK100 are very close to the measured d_{V95}, see Table S2: 43 μm vs 36 ± 4 μm for AK10; 65 μm vs 58 ± 8 μm for AK100. However, higher values are predicted for AK1000 and AK30000: 257 μm vs 130 ± 60 μm for AK1000 and 3080 μm vs 550 ± 70 μm showing again that for more viscous oils the decreased viscosity during the emulsification has to be considered. Note that in our previous study [11] we used Eq. (11) to describe the experimental data obtained with various oils having plateau viscosity up to 500 mPa.s. Very good agreement between predicted and measured drop diameters were established for oils with viscosity up to 200 mPa.s whereas a noticeable smaller in size drops are formed from silicone oil with 500 mPa.s compared to predicted ones, see Fig. 7 in [11], showing that the shear thinning of viscous oil becomes important for oils with viscosity above 200 mPa.s.

We used two approaches to account for possible shear thinning of the oil phase during drop breakage. In the first approach, we assume that η_D in Eq. (11) can be replaced by $\eta_{d\omega}$ determined from DWS measurements at $\omega = 1.9 \times 10^4$ rad/s. This approach assumes that the shear rate inside the breaking drop is equal to the global shear rate estimated to be 1.9×10^4 s^{-1}. The determined results for $d_{I\omega}$ are given in Table S2. One sees excellent agreement between experimentally measured and theoretically predicted drop sizes even for the viscous oils.

The second approach accounts for the shear-thinning of the viscous oils. It assumes the viscosity of the drop decreases with the shear rate but instead of using the global shear rate, a local shear rate inside breaking drop is estimated as $C_6\frac{(\varepsilon d_I)^{\frac{1}{3}}}{d_I}$. Incorporating Eq. (1) into Eq. (11) we derive the drop size in the inertial regime for oils with shear-thinning behavior:

$$C_1 C_2 \rho_C (\varepsilon d_I)^{2/3} = C_4 \frac{\sigma}{d_I} + C_5 \left(\frac{\eta_{D0} - \eta_{D\infty}}{1 + \left(C_6 k_D \frac{(\varepsilon d_I)^{1/3}}{d_I} \right)^{n_D}} + \eta_{D\infty} \right) C_6 \frac{(\varepsilon d_I)^{1/3}}{d_I} \quad (12)$$

d_I is the maximal stable drop diameter in the inertial regime of emulsification based on the force requirement, η_{D0}, $\eta_{D\infty}$, k_D and n_D are the parameters for rheological response of oily phase with non-Newtonian response, C_6 is an unknown constant accounting for the ratio between the shear rate inside the dispersed phase and in the continuous phase. Assuming that $C_6 = 0.8$ we obtain reasonable agreement for the measured drop sizes for all silicone emulsions in 1.25 wt% PVA, see Table S2. Note that the calculated values for d_I using Eq. (12) are very close to values calculated by using $\eta_{d\omega}$ in Eq. (11) showing that both approaches account reasonably for the shear-thinning behavior of viscous oils.

In the viscous turbulent regime, where the drops break due to viscous forces inside the smallest turbulent eddies the viscosity of the continuous phase becomes important. One way to account for this importance is to use the "Grace plot" [14,66,67], which represents the critical capillary number for the largest stable drops in the formed emulsions, $Ca_{CR} = \eta_C \dot{\gamma} d_{V95}/\sigma$, as a function of the viscosity ratio, $p = \eta_D/\eta_C$. According to the Grace plot the drops with a diameter larger than that corresponding to the Ca_{CR}, should be broken into smaller drops by the viscous stress of the sheared medium, whereas the smaller drops would remain unbroken, due to the drop capillary pressure opposing drop deformation. The experimental data for d_{V95} formed in a turbulent viscous regime are used to construct the plot shown in Fig. S5. Note that viscosities of dispersed and continuous phases measured for zero-shear viscosity (Fig. S5A), and for the complex viscosity in DWS at $\omega = 1.9 \times 10^4$ rad/s (Fig. S5B) are used for the construction of these plots. As can be seen, the experimental data do not follow a single master curve in either case. The experimental results are closer to each other when the viscosities measured in DWS are used but still, a deviation that exceeds one order of magnitude is observed at some viscosity ratios.

In a previous publication [21] we showed that the maximal drop diameter in the viscous turbulent regime can describe the data obtained with two mineral oils with different viscosities of 19 and 36 mPa.s:

$$d \approx a \frac{\sigma}{(\varepsilon \eta_C \rho_C)^{1/2}} \quad (13)$$

where a is a coefficient accounting for the viscosity ratio. Constant a was found to be 0.9 for triglyceride oil with a viscosity of 19 mPa.s and 1.14 for a more viscous one with a viscosity of 36 mPa.s. In Fig. S6 we replotted the experimental data obtained in the viscous turbulent regime according to Eq. (13). It implies that the viscous stress inside the smallest eddies is responsible for drop breakage. One sees that the data are largely scattered due to BS solutions, whose thinning affects the the viscosity of the continious phase. The effect is less pronounced for emulsions prepared in PVA solutions, but variation is still visible, especially for more viscous oils.

In another study [13], we demonstrated that the outcome of emulsification does not depend on the interfacial tension for concentrated emulsions. To explore this hypothesis further, we standardized the interfacial tension in Eq. (13) at 40 mN/m, corresponding to the interfacial tension of the bare silicone oil-water interface. The results indicate that emulsions prepared with different silicone oils display varying values of the correction coefficient a, even when the interfacial tension is assumed constant. Another reason for this check was that existing methods for measuring interfacial tension can only measure it on a time scale above 1 s (see Fig. 2 above), whereas the typical time scale for drop breakage is in the millisecond range. This suggests that the actual interfacial tension could be higher than the measured value. The highest possible value corresponds to the pure water-oil interface, which is why this check was performed. However, as can be seen, a constant interfacial tension cannot explain the results obtained with different silicone oils in a given solution.

In Eq. (13) the opposing forces are only those related to the action of surface tension but the effect of viscous dissipation inside the breaking drop is not accounted for. To account for this effect, we assume that the viscous stress inside the breaking drop can be expressed as in the case of inertial regime [8]:

$$\tau_D = \eta_D C_6 \frac{(\varepsilon d_V)^{1/3}}{d_V} \quad (14)$$

The driving force for drop breakage in the turbulent viscous regime is the shear stress inside the smallest eddies which is expressed as:

$$\tau_C = \eta_C C_2^{1/2} \frac{(\varepsilon\lambda_0)^{1/3}}{\lambda_0} \tag{15}$$

To account for the shear thinning of the continuous and dispersed phases we introduced Eq. (1) in Eqs. (14) and (15). To determine the maximal stable drop diameter in turbulent viscous regime, we assume that the viscous forces acting in the smallest turbulent eddies have to be higher than the opposing forces for drop breakage as in the inertial regime: capillary force and viscous force inside the breaking drop. The following expression is proposed for the estimation of the drop size in the viscous turbulent regime:

$$\left(\frac{\eta_{C0}-\eta_{C\infty}}{1+\left(k_C C_2^{1/2}\frac{(\varepsilon\lambda_0)^{1/3}}{\lambda_0}\right)^{n_C}}+\eta_{C\infty}\right) C_2^{1/2}\frac{(\varepsilon\lambda_0)^{1/3}}{\lambda_0} = C_7\frac{\sigma}{d_V} + C_8\left(\frac{\eta_{D0}-\eta_{D\infty}}{1+\left(k_D C_6\frac{(\varepsilon d_V)^{1/3}}{d_V}\right)^{n_D}}+\eta_{D\infty}\right) C_6\frac{(\varepsilon d_V)^{1/3}}{d_V} \tag{16}$$

where λ_0 is determined from Eq. (6) values of η_{C0}, $\eta_{C\infty}$, k_C, n_C, η_{D0}, $\eta_{D\infty}$, k_D, n_D are given in Table 1, d_V is the drop size in the viscous regime. The values of constants are $C_2 = 2.0$ [62], $C_6 = 0.8$; $C_7 = 0.5$; $C_8 = 0.015$. The predicted drop sizes in the inertial regime by Eq. (12) and in the viscous regime by Eq. (16) are shown in Fig. 4 as a function of the experimentally measured maximal drop sizes. One sees that the description is good for all studied systems, including BS solutions with different salt concentrations. The comparison between Eqs. (16) and (12) shows that the opposing forces for drop breakage in both regimes are similar (surface tension forces and viscous force inside breaking drop) but their contribution is different. The value of C_7 used for the viscous regime is two times smaller than C_4 (0.5 vs 1.089), used for the inertial regime with the latter showing that the surface tension force has smaller effect on the drop breakage in the viscous regime compared to inertial regime. The value of C_5 is 19-fold higher than the value of C_8 (0.285 vs 0.015) accounting for much easier drop breakage of highly viscous oils in viscous turbulent regime. In the viscous regime, the relative contribution of the viscous dissipation inside the breaking drops is much smaller compared to the capillary force, whereas this effect is less pronounced in the inertial regime. However, even in the viscous regime, the breakage of the emulsion drops with low viscosity, e.g. AK10, is dominated by the capillary pressure, whereas the most viscous oil (e.g. AK30000) is dominated by the viscous stress inside the breaking drop and interfacial tension plays a negligible role.

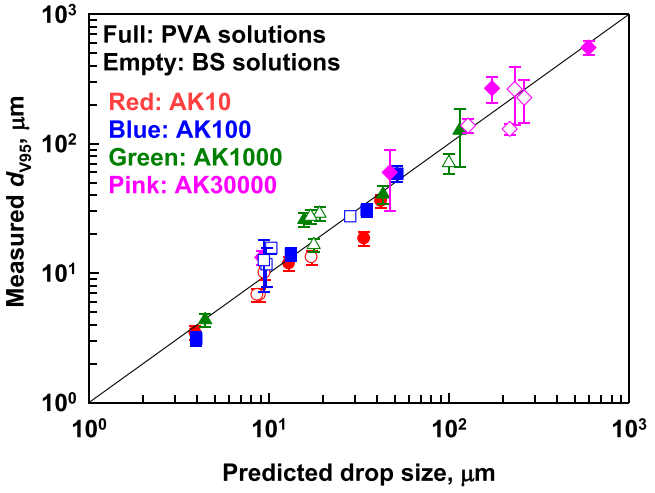

Fig. 4. Experimentally determined values of d_{V95}, and calculated via Eq. (10) for emulsions formed in inertial regime and Eq. (16) for emulsions formed in viscous regime with constants determined in the current study for viscous regime of $C_6 = 0.8$; $C_7 = 0.7$; $C_8 = 0.015$ and constantans known from the literature for inertial regime: $C_1 = 0.7$ [62], $C_2 = 2.0$ [62], $C_4 = 1.089$ [11]; $C_5 = 0.285$ [11].

4. Conclusions

We investigated both experimentally and theoretically the emulsification of silicone oils in nearly Newtonian polyvinyl alcohol (PVA) solutions and non-Newtonian worm-like micellar solutions (BS+NaCl). We hypothesized that emulsification in both Newtonian and non-Newtonian media in the turbulent regime could be predicted after accounting for shear thinning of both the dispersed and continuous phases. This hypothesis was confirmed through the development of a theoretical model that considers the local shear rates in the turbulent eddies, leading to reduced viscosities within the drop and aqueous phases. This model allows a significant improvement in the drop size predictions and extends the current frontier in emulsification.

The new model shows that the complex interplay occurs between interfacial tension and oil viscosity in viscous turbulent regime of emulsification. Namely, the interfacial tension plays a key role in the emulsification of less viscous oils (0.01 Pa.s), whereas the emulsification of more viscous oils ($\geq$ 1 Pa.s) is significantly affected by the viscous dissipation inside the breaking drops. This interplay has not been demonstrated previously for rotor-stator devices [6,8–13,17–24,65], especially in the case of shear-thinning fluids. The extended use of diffusive wave spectroscopy (DWS) for the characterization of the viscosity at high shear rates improved model accuracy up to 8–10 times for the viscous oils and its use has the potential to improve results interpretation beyond semi-empirical fits that were previously used to treat the data [13]. The improvement is even more pronounced for worm-like micellar solutions and concentrated PVA solutions.

The new theoretical model, along with the proposed methodology for accounting for viscosity at high shear rates, provides pathways for improving emulsification efficiency in high-shear devices, industrial formulations that require more monodisperse drops, and even in computational fluid dynamics (CFD) simulations that model the drop breakage. Some of these aspects are particularly important in cosmetic applications, which exploit worm-like micelles or perhaps even structured gel phases that occur with variations in surfactant concentration or processing temperature.

CRediT authorship contribution statement

Slavka Tcholakova: Writing – review & editing, Visualization, Software, Methodology, Funding acquisition, Formal analysis, Conceptualization. **Ivan Lesov:** Writing – original draft, Methodology, Investigation, Data curation.

Funding

This study is financed by the European Union-Next Generation EU, through the National Recovery and Resilience Plan of the Republic of Bulgaria, Project no. BG-RRP-2.004-0008-C01.

Abbreviations

AK10, AK100, AK1000, AK30000	silicone oils with varying viscosities
BS	mixture of Sodium Laureth Sulfate (SLES) and Cocoamidopropyl Betaine (CAPB)
DSA	Drop-Shape Analysis
DVT	Drop Volume Tensiometer
DWS	Diffusive Wave Spectroscopy
FDDM	Fast Deformed Drop Method
PDMS	Polydimethylsiloxane
PVA	Polyvinyl Alcohol
PDI	Polydispersity Index

Greek Symbols

ε	energy dissipation per unit mass of fluid
$\dot{\gamma}$	shear rate
$\dot{\gamma}_{\lambda 0}$	shear rate inside the smallest turbulent eddies
$\dot{\gamma}_{\lambda 01}$	calculated by Eq. (3) using λ_{01}
$\dot{\gamma}_{\lambda P}$	calculated by Eq. (3) using λ_P
$\dot{\gamma}_{\lambda \omega}$	calculated by Eq. (3) using λ_ω
λ_0	size of the smallest eddies in turbulent flow
λ_{01}	calculated by Eq. (6) accounting for shear thinning behavior of continuous phase
λ_ω	calculated by Eq. (7) assuming constant viscosity of the continuous phase measured by DWS at $\omega = 1.9 \times 10^4$ rad/s
λ_P	calculated by Eq. (7) assuming constant viscosity of the continuous phase measured by rheometer at plateau region
η_C	viscosity of the continuous phase
η_{C0}	zero-shear viscosity determined from the best fit of experimental data with Eq. (1)
$\eta_{C\infty}$	viscosity at high shear rate determined from the best fit of experimental data with Eq. (1)
η_{CP}	zero-shear viscosity of the continuous phase measured by rheometer
η_D	viscosity of the dispersed phase
η_{D0}	zero-shear viscosity determined from the best fit of experimental data with Eq. (1)
$\eta_{D\infty}$	viscosity at high shear rate determined from the best fit of experimental data with Eq. (1)
η_{DP}	zero-shear viscosity of the dispersed phase measured by rheometer
η_ω	complex viscosity as measured via DWS
$\eta_{c\omega}$	complex viscosity of the continuous phase at $\omega = 1.9 \times 10^4$ rad/s
$\eta_{d\omega}$	complex viscosity of the dispersed phase at $\omega = 1.9 \times 10^4$ rad/s
σ	interfacial tension
τ_D	viscous stress inside drops
τ_C	viscous stress inside the smallest eddies
ρ_C, ρ_D	mass density of the continuous phase and the dispersed phase
ω	frequency from diffusive wave spectrometer (DWS)

Latin Symbols

a	constant for drop breakage efficiency in turbulent viscous regime, accounting for the viscosity ratio
b_1	constant related to the energy dissipation rate in a homogenizer
d_V	maximum stable drop diameter in viscous regime
d_{V95}	Experimentally determined maximum drop diameter by volume
d_{V50}	median drop diameter by volume
d_I	maximal stable drop diameter in inertial regime
$d_{IMIN\omega}$	assuming high-shear viscosity, as measured by DWS
d_{MINP}	assuming zero-shear viscosity, as measured via rheometer
d_{MINI}	minimum drop size that can be deformed during the lifespan of the eddies with similar size
k_C, k_D	characteristic time constants for continuous and dispersed phases, as in the Cross rheological model
l	gap distance between rotor and stator
t_{DEF}	deformation time in inertial regime
t_{EDDY}	lifetime of eddies
r	rotor radius
p	viscosity ratio, η_D/η_c
C1, C2, C3, C4, C5, C6, C7, C8	numerical constants for the different regimes of emulsification
Ca_{CR}	critical capillary number
L	rotor diameter
N	rotor rotational speed
ΔP_T	Pressure fluctuations related to turbulence
U	fluid velocity

Declaration of Competing Interest

The authors declare that they have no known competing financial interests or personal relationships that could have appeared to influence the work reported in this paper.

Acknowledgment

The authors thank Mrs. Dora Dimitrova for her help with some of the interfacial tension measurements.

Appendix A. Supporting information

Supplementary data associated with this article can be found in the online version at doi:10.1016/j.colsurfa.2024.135603.

Data availability

Data will be made available on request.

References

[1] A. Gupta, H.B. Eral, T.A. Hatton, P.S. Doyle, Nanoemulsions: formation, properties and applications, Soft Matter 12 (2016) 2826, https://doi.org/10.1039/c5sm02958a.
[2] R. Pal, Rheology of simple and multiple emulsions, Curr. Opin. Colloid Interface Sci. 16 (2011) 41–60, https://doi.org/10.1016/j.cocis.2010.10.001.
[3] N.I. Politova, S. Tcholakova, S. Tsibranska, N.D. Denkov, K. Muelheims, Coalescence stability of water-in-oil drops: effects of drop size and surfactant concentration, Colloids Surf. A 531 (2017) 32–39, https://doi.org/10.1016/j.colsurfa.2017.07.085.
[4] G. Sala, F. van de Velde, M.A. Cohen Stuart, G.A. van Aken, Oil droplet release from emulsion-filled gels in relation to sensory perception, Food Hydrocoll. 21 (2007) 977–985, https://doi.org/10.1016/j.foodhyd.2006.08.009.
[5] S. Tcholakova, N.D. Denkov, I.B. Ivanov, B. Campbell, Coalescence stability of emulsions containing globular milk proteins, Adv. Colloid Interface Sci. 123–126 (2006) 259–293, https://doi.org/10.1016/j.cis.2006.05.021.
[6] P. Walstra, Formation of emulsions, in: Encyclopedia of Emulsion Technology, Marcel Dekker, New York, 1983 (Chapter 2).
[7] P. Walstra, T.J. Geurts, A. Noomen, A. Jellema, M.A.J.S. van Boekel, Dairy Technology, Marcel Decker, New York, 1999.
[8] J.T. Davies, Drop sizes of emulsions related to turbulent energy dissipation rates, Chem. Eng. Sci. 40 (1985) 839, https://doi.org/10.1016/0009-2509(85)85036-3.
[9] A.N. Kolmogoroff, Drop breakage in turbulent flow, Compt. Rend. Acad. Sci. URSS 66 (1949) 825.
[10] J.O. Hinze, Fundamentals of the hydrodynamic mechanism of splitting in dispersion processes, AIChE J. 1 (1955) 289, https://doi.org/10.1002/aic.690010303.
[11] N. Vankova, S. Tcholakova, N.D. Denkov, I.B. Ivanov, V.D. Vulchev, T. Danner, Emulsification in turbulent flow: 1. Mean and maximum drop diameters in inertial and viscous regimes, J. Colloid Interface Sci. 312 (2007) 363–380, https://doi.org/10.1016/j.jcis.2007.03.059.
[12] V. Cristini, J. Blawzdziewicz, M. Loewenberg, L.R. Collins, Breakup in stochastic Stokes flows: sub-Kolmogorov drops in isotropic turbulence, J. Fluid Mech. 492 (2003) 231, https://doi.org/10.1017/S0022112003005561.
[13] S. Tcholakova, I. Lesov, K. Golemanov, N. Denkov, S. Judat, R. Engel, T. Daner, Efficient emulsification of viscous oils at high drop volume fraction, Langmuir 27 (2011) 14783–14796, https://doi.org/10.1021/la203474b.
[14] K.M.B. Jansen, W.G.M. Agterof, J. Mellema, Droplet breakup in concentrated emulsions, J. Rheol. 45 (2001) 227, https://doi.org/10.1039/C3SM51843D.

[15] T.G. Mason, J. Bibette, Shear rupturing of droplets in complex fluids, Langmuir 13 (1997) 4600–4613, https://doi.org/10.1021/la9700580.
[16] T.G. Mason, J. Bibette, Emulsification in viscoelastic media, Phys. Rev. Lett. 77 (1996) 3481, https://doi.org/10.1103/PhysRevLett.77.3481.
[17] S. Tcholakova, N.D. Denkov, D. Hristova, M. Deruelle, Emulsification and emulsion stability of silica-charged silicone oils, in: Proceedings of the 5th World Congress on Emulsions, Lyon, France, Paper No. 4.1-50, 2010.
[18] E. Akiyama, A. Kashimoto, H. Hotta, T. Kitsuki, Mechanism of oil-in-water emulsification using a water-soluble amphiphilic polymer and lipophilic surfactant, J. Colloid Interface Sci. 300 (2006) 141–148, https://doi.org/10.1016/j.jcis.2006.03.066.
[19] E. Akiyama, A. Kashimoto, K. Fukuda, H. Hotta, T. Suzuki, T. Kitsuki, Thickening properties and emulsification mechanisms of new derivatives of polysaccharides in aqueous solution, J. Colloid Interface Sci. 282 (2005) 448–457, https://doi.org/10.1016/j.jcis.2004.08.178.
[20] C. Rouzes, A. Durand, M. Leonard, E. Dellacherie, Surface activity and emulsification properties of hydrophobically modified dextrans, J. Colloid Interface Sci. 253 (2002) 217–223, https://doi.org/10.1006/jcis.2002.8357.
[21] D. Gazolu-Rusanova, I. Lesov, S. Tcholakova, N. Denkov, B. Ahtchi, Food grade nanoemulsions preparation by rotor-stator homogenization, Food Hydrocoll. 102 (2020) 105579, https://doi.org/10.1016/j.foodhyd.2019.105579.
[22] D.J. McClements, Biopolymers in food emulsions, in: Modern Biopolymer Science: Bridging the Divide between Fundamental Treatise and Industrial Application, Academic Press, 2009, pp. 129–166.
[23] M.S. Rodrıguez, L.A. Albertengo, E. Agulló, Emulsification capacity of chitosan, Carbohydr. Polym. 48 (2002) 271–276, https://doi.org/10.1016/S0144-8617(01)00258-2.
[24] D.J. McClements, C.E. Gumus, Natural emulsifiers — biosurfactants, phospholipids, biopolymers, and colloidal particles: molecular and physicochemical basis of functional performance, Adv. Colloid Interface Sci. 234 (2016) 3–26, https://doi.org/10.1016/j.cis.2016.03.002.
[25] R. Pal, Rheological behaviour of concentrated surfactant solutions and emulsions, Colloids Surf. 64 (1992) 207–215, https://doi.org/10.1016/0166-6622(92)80101-7.
[26] D.P. Acharya, H. Kunieda, Wormlike micelles in mixed surfactant solutions, Adv. Colloid Interface Sci. 123–126 (2006) 401–413, https://doi.org/10.1016/j.cis.2006.05.024.
[27] Z. Chu, C.A. Dreiss, Y. Feng, Smart wormlike micelles, Chem. Soc. Rev. 42 (2013) 7174–7203, https://doi.org/10.1039/C3CS35490C.
[28] M. Pleines, W. Kunz, T. Zemb, D. Benczédi, W. Fieber, Molecular factors governing the viscosity peak of giant micelles in the presence of salt and fragrances, J. Colloid Interface Sci. 537 (2019) 682–693, https://doi.org/10.1016/j.jcis.2018.11.072.
[29] Z. Mitrinova, H. Alexandrov, N. Denkov, S. Tcholakova, Effect of counter-ion on rheological properties of mixed surfactant solutions, Colloids Surf. A 643 (2022) 128746, https://doi.org/10.1016/j.colsurfa.2022.128746.
[30] Z. Mitrinova, S. Tcholakova, N. Denkov, Control of surfactant solution rheology using medium-chain cosurfactants, Colloids Surf. A 537 (2018) 173–184, https://doi.org/10.1016/j.colsurfa.2017.10.018.
[31] H. Wu, S. Shu, N. Yang, G. Lian, S. Zhu, M. Liu, Modeling of power characteristics for multistage rotor–stator mixers of shear-thinning fluids, Chem. Eng. Sci. 117 (2014) 173–182, https://doi.org/10.1016/j.ces.2014.06.039.
[32] Y. Ji, E. Missi, J. Bellettre, T. Burghelea, A. Montillet, P. Massoli, Dynamics of a Newtonian droplet in the turbulent flow of a shear thinning fluid in a microchannel, Phys. Rev. Fluids 8 (2023) 043301, https://doi.org/10.1103/PhysRevFluids.8.043301.
[33] D. Qiu, L. Silva, A.L. Tonkovich, R. Arora, Micro-droplet formation in non-Newtonian fluid in a microchannel, Microfluid. Nanofluid. 8 (2010) 531–548, https://doi.org/10.1007/s10404-009-0487-5.
[34] A.K. Wacker Silicone Fluids. Retrieved from ⟨https://www.behlke.com/pdf/wacker_silicone_oil.pdf⟩ (Accessed 04 June 2024).
[35] Maxon Bartley, Starch Michael, Formulating skin care products with silicones: approaches and strategies, in: Handbook of Formulating Dermal Applications: A Definitive Practical Guide. Nava Dayan, Scrivener Publishing LLC, New York, USA, 2017. ⟨https://repository.poltekkes-kaltim.ac.id/1181/1/26.%20Handbook_of_Formulating_Dermal_Applications.pdf⟩.
[36] H. Nazir, W. Zhang, Y. Liu, X. Chen, L. Wang, M.M. Naseer, G. Ma, Silicone oil emulsions: strategies to improve their stability and applications in hair care products, Int. J. Cosmet. Sci. 36 (2014) 124–133, https://doi.org/10.1111/ics.12104.
[37] J. Anthony, O'Lenick Jr. Silicones for Personal Care, 2nd Edition, Allured Publishing Corporation, 2008. ⟨https://scientificspectator.com/documents/book%20service/Anthony%20O'Lenick%20Silicones%20for%20Personal%20Care.pdf⟩.
[38] Zhenhua Hu, Meiling Liao, Yinghui Chen, Yunpeng Cai, Lele Meng, Yajun Liu, Nan Lv, Zhenguo Liu, Weien Yuan, A novel preparation method for silicone oil nanoemulsions and its application for coating hair with silicone, Int. J. Nanomed. 7 (2012) 5719–5724, https://doi.org/10.2147/IJN.S37277.
[39] Habiba Nazir, Piping Lv, Lianyan Wang, Guoping Lian, Shiping Zhu, Guanghui Ma, Uniform-sized silicone oil microemulsions: preparation, investigation of stability and deposition on hair surface, J. Colloid Interface Sci. 364 (2011) 56, https://doi.org/10.1016/j.jcis.2011.07.096.
[40] W.P. Cox, E.H. Merz, Correlation of dynamic and steady flow viscosities, J. Polym. Sci. 28 (1958) 619, https://doi.org/10.1002/pol.1958.1202811812.
[41] C.M. Roland, Rheological behavior and processing of unvulcanized rubber, in: B. Erman, J.E. Mark (Eds.), The Science and Technology of Rubber, Fourth Edition, Academic Press, USA, 2013, https://doi.org/10.1016/B978-012464786-2/50009-2.
[42] D.W. Mead, Analytic derivation of the Cox–Merz rule using the MLD "toy" model for polydisperse linear polymers, Rheol. Acta 50 (2011) 837–866, https://doi.org/10.1007/s00397-011-0550-5.
[43] K.C. Tam, C. Tiu, Steady and dynamic shear properties of aqueous polymer solutions, J. Rheol. 33 (1989) 257, https://doi.org/10.1122/1.550015.
[44] O. Manero, F. Bautista, J.F.A. Soltero, J.E. Puig, Dynamics of worm-like micelles: the Cox–Merz rule, J. Non-Newton. Fluid Mech. 106 (2002) 1–15, https://doi.org/10.1016/S0377-0257(02)00082-4.
[45] S.E. Quintana, M. Zuñiga-Navarro, D. Ramirez-Brewer, L.A. García-Zapateiro, Applicability of the Cox–Merz relationship for mayonnaise enriched with natural extracts, Fluids 8 (2023) 287, https://doi.org/10.3390/fluids8110287.
[46] J.D. Mata-Mota, J.A. Gallegos-Infante, J.D. Pérez-Martínez, N.E. Rocha-Guzmán, R. F. González-Laredo, Effect of hydrogel/oleogel ratio, speed and time of mixing, on the mechanical properties of bigel materials and the application of Cox-Merz rule, Food Mater. Res. 3 (2023) 24, https://doi.org/10.48130/FMR-2023-0024.
[47] R.G. Larson, The Structure and Rheology of Complex Fluids, Oxford University Press, New York, 1999.
[48] T.S.R. Al-Hadithi, H.A. Barnes, K. Walters, The relationship between the linear (oscillatory) and nonlinear (steady-state) flow properties of a series of polymer and colloidal systems, Colloid Polym. Sci. 270 (1992) 40–46, https://doi.org/10.1007/BF00656927.
[49] C. Carotenuto, G. Rexha, R. Martone, M. Minale, The microstructural change causing the failure of the Cox–Merz rule in Newtonian suspensions: experiments and simulations, Rheol. Acta 60 (2021) 309–325, https://doi.org/10.1007/s00397-021-01270-8.
[50] T. Kaully, A. Siegmann, D. Shacham, Rheology of highly filled natural CaCO3 composites. II. Effects of solid loading and particle size distribution on rotational rheometry, Polym. Compos. (2007), https://doi.org/10.1002/pc.20309.
[51] Z. Kőkuti, K. van Gruijthuijsen, M. Jenei, G. Tóth-Molnár, A. Czirják, J. Kokavecz, P. Ailer, L. Palkovics, A.C. Völker, G. Szabó, High-frequency rheology of a high viscosity silicone oil using diffusing wave spectroscopy, Appl. Rheol. 24 (2014) 63984, https://doi.org/10.3933/ApplRheol-24-63984.
[52] D. Parisi, C.D. Ditillo, A. Han, S. Lindberg, M.W. Hamersky, R.H. Colby, Rheological investigation on the associative properties of poly(vinyl alcohol) solutions, J. Rheol. 66 (2022) 1141–1150, https://doi.org/10.1122/8.0000435.
[53] X. Chen, Y. Zhang, H. Wang, S.-W. Wang, S. Liang, R.H. Colby, Solution rheology of cellulose in 1-butyl-3-methyl imidazolium chloride, J. Rheol. 55 (2011) 485–494, https://doi.org/10.1122/1.3553032.
[54] Y. Caram, F. Bautista, J.E. Puig, O. Manero, On the rheological modeling of associative polymers, Rheol. Acta 46 (2006) 45–57, https://doi.org/10.1007/s00397-005-0066-y.
[55] W. Zou, G. Tan, H. Jiang, K. Vogtt, M. Weaver, P. Koenig, G. Beaucage, R.G. Larson, From well-entangled to partially-entangled wormlike micelles, Soft Matter 15 (2019) 642–655, https://doi.org/10.1039/c8sm02223b.
[56] N.A. Spenley, M.E. Cates, T.C.B. McLeish, Nonlinear rheology of wormlike micelles, Phys. Rev. Lett. 71 (1993) 939–942, https://doi.org/10.1103/PhysRevLett.71.939.
[57] S.E. Anachkov, G.S. Georgieva, L. Abezgauz, D. Danino, P.A. Kralchevsky, Viscosity peak due to shape transition from wormlike to disklike micelles: effect of dodecanoic acid, Langmuir 34 (2018) 4897–4907, https://doi.org/10.1021/acs.langmuir.8b00421.
[58] M.M. Cross, Rheology of non-Newtonian fluids: a new flow equation for pseudoplastic systems, J. Colloid Sci. 20 (5) (1965) 417–437, https://doi.org/10.1016/0095-8522(65)90022-X.
[59] D.V. Boger, Demonstration of upper and lower Newtonian fluid behavior in a pseudoplastic fluid, Nature 265 (1977) 126–128, https://doi.org/10.1038/265126a0.
[60] R. Miller, K.-H. Schano, A. Hofmann, Hydrodynamic effects in measurements with the drop volume technique at small drop times 1. Surface tensions of pure liquids and mixtures, Colloids Surf. A Physicochem. Eng. Asp. 92 (1994) 189–196, https://doi.org/10.1016/0927-7757(94)02945-8.
[61] R. Miller, M. Bree, V.B. Fainerman, Hydrodynamic effects in measurements with the drop volume technique at small drop times-3. Surface tensions of viscous liquids, Colloids Surf. A Physicochem. Eng. Asp. 142 (1998) 237–242, https://doi.org/10.1016/S0927-7757(98)00240-4.
[62] G.K. Batchelor, An Introduction to Fluid Dynamics, Cambridge University Press, 1967.
[63] Daniele L. Marchisio, Miroslav Soos, Jan Sefcik, Massimo Morbidelli, Role of turbulent shear rate distribution in aggregation and breakage processes, AIChE J. 52 (2005) 158, https://doi.org/10.1002/aic.10614.
[64] Moon Joo Lee, John Kim, Parviz Moin, Structure of turbulence at high shear rate, J. Fluid Mech. 216 (1990) 561–583, https://doi.org/10.1017/S0022112090000532.
[65] S. Tcholakova, N. Vankova, N.D. Denkov, T. Danner, Emulsification in turbulent flow: 3. Daughter drop-size distribution, J. Colloid Interface Sci. 310 (2007) 570–589, https://doi.org/10.1016/j.jcis.2007.01.097.
[66] H.P. Grace, Dispersion phenomena in high viscosity immiscible fluid systems and application of static mixers as dispersion devices in such systems, Chem. Eng. Commun. 14 (1982) 225, https://doi.org/10.1080/00986448208911047.
[67] M. Loewenberg, E.J. Hinch, Numerical simulation of a concentrated emulsion in shear flow, J. Fluid Mech. 321 (1996) 395, https://doi.org/10.1017/S002211209600777X.